Electronic Supplementary Material (ESI) for Nanoscale.

Supplementary Information

Defect Creation in WSe_2 with Microsecond Photoluminescence Lifetime by Focused Ion Beam Irradiation

Qingkai Qian,[a] Lintao Peng,[b] Nestor Perea-Lopez,[c,d] Kazunori Fujisawa,[c,d] Kunyan Zhang,[a] Xiaotian Zhang,[e] Tanushree H. Choudhury,[f] Joan M. Redwing,[e, f] Mauricio Terrones,[c,d,e,f,g] Xuedan Ma[b] and Shengxi Huang[a]*

[a]Department of Electrical Engineering, The Pennsylvania State University, University Park, Pennsylvania 16802, United States

[b]Center for Nanoscale Materials, Argonne National Laboratory, Argonne, Illinois 60439, United States

[c]Department of Physics, The Pennsylvania State University, University Park, Pennsylvania 16802, United States

[d]Center for 2-Dimensional and Layered Materials, The Pennsylvania State University, University Park, Pennsylvania 16802, United States

[e]Department of Materials Science and Engineering , The Pennsylvania State University, University Park, Pennsylvania 16802, United States

[f]2D Crystal Consortium, The Pennsylvania State University, University Park, Pennsylvania 16802, United States

[g]Department of Chemistry, The Pennsylvania State University, University Park, Pennsylvania 16802, United States

* Email: sjh5899@psu.edu

Table S1 Basic settings of FEI Helios NanoLab 660 dual beam instrument during FIB irradiation

Scanning parameters	Value
Ion type	Ga^+, normal incidence
Beam current	1.1, 7.7 or 230 pA
Accelerating voltage	30 kV
Dwell Time	50.0 ns
Step size	135 nm (260 nm)
Scanning size	410 μm×274 μm
Frame Time	0.3 s (0.08s)

Table S2 Controlled irradiation parameters to generate defects with densities ranging over four orders of magnitude

Beam current	Scanning Frame No.	Step size	Ion Dose
1.1 pA	2	260 nm	1.0×10^{9} cm^{-2}
7.7 pA	1	135 nm	1.3×10^{10} cm^{-2}
7.7 pA	7	135 nm	0.9×10^{11} cm^{-2}
7.7 pA	72	135 nm	0.9×10^{12} cm^{-2}
230 pA	26	135 nm	1.0×10^{13} cm^{-2}

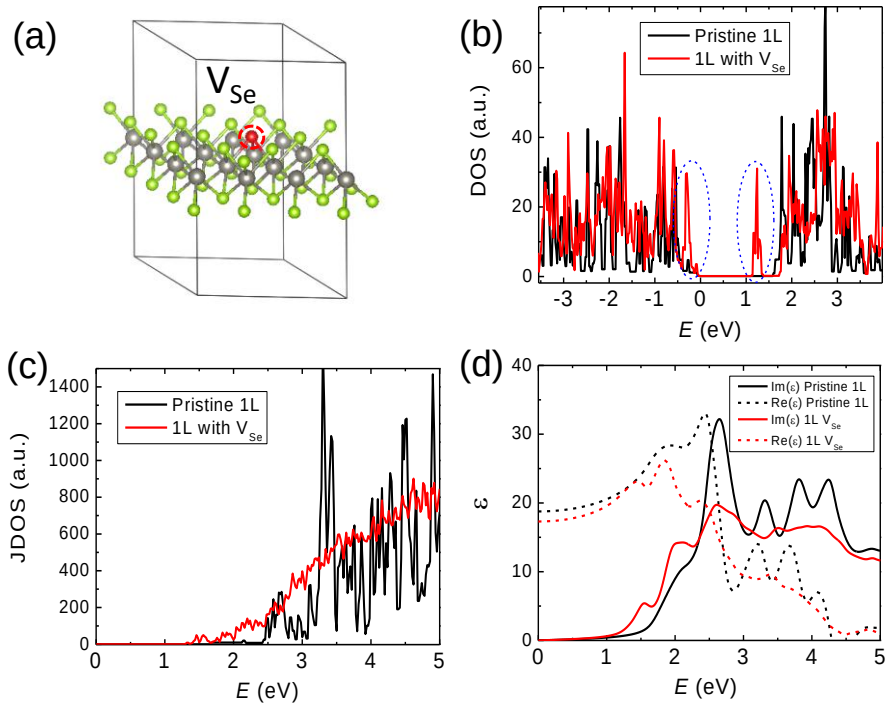

Fig. S1 (a) Atomic structure of 1L WSe_2 in 3×3 unitcell with single Se vacancy. (b) Calculated density of states (DOS), compared with pristine WSe_2, defect states are introduced by vacancy and are indicated by the blue circles. The upper defect levels are within the bandgap and close to the conduction band, which is consist with the electronic band structure shown in the manuscript.

(c) Joint density of states of 1L WSe_2 with single Se vacancy. More joint states with lower energy are introduced by the Se vacancy, which can result in transitions, electron/hole recombinations and photon emissions with lower energy during and after optical excitation, as reflected by the larger imaginary permittivity in the low-energy range in (d).

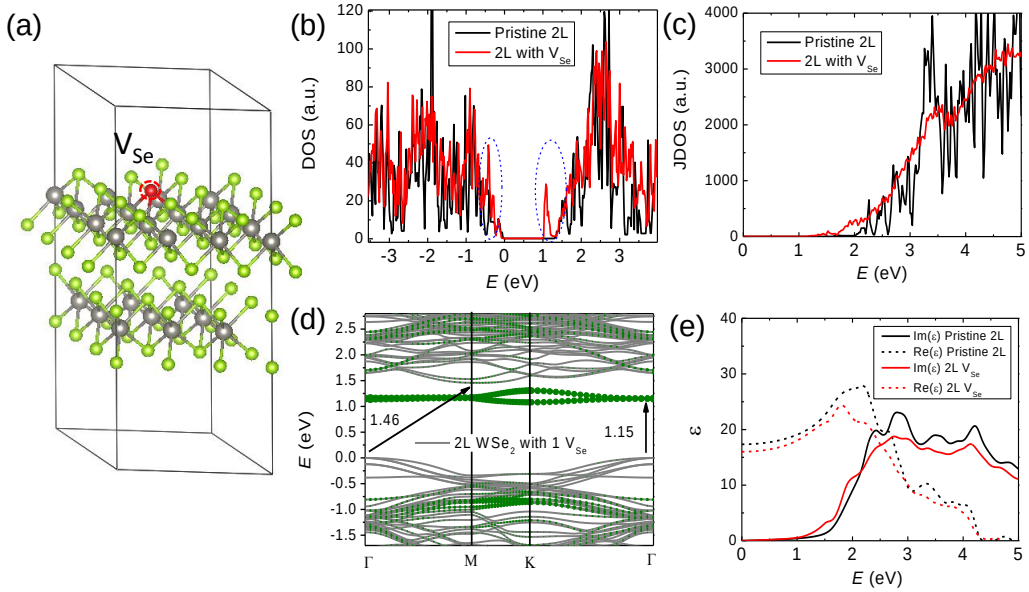

Fig. S2 (a) Atomic structure of 2L WSe_2 in 3×3 unitcell with single Se vacancy. (b) Calculated density of states (DOS), (c) joint density of states (JDOS), (d) band structure and (e) permittivity. Compared with single-layer WSe_2, the Se vacancy in 2L WSe_2 causes milder changes in the JDOS and permittivity.

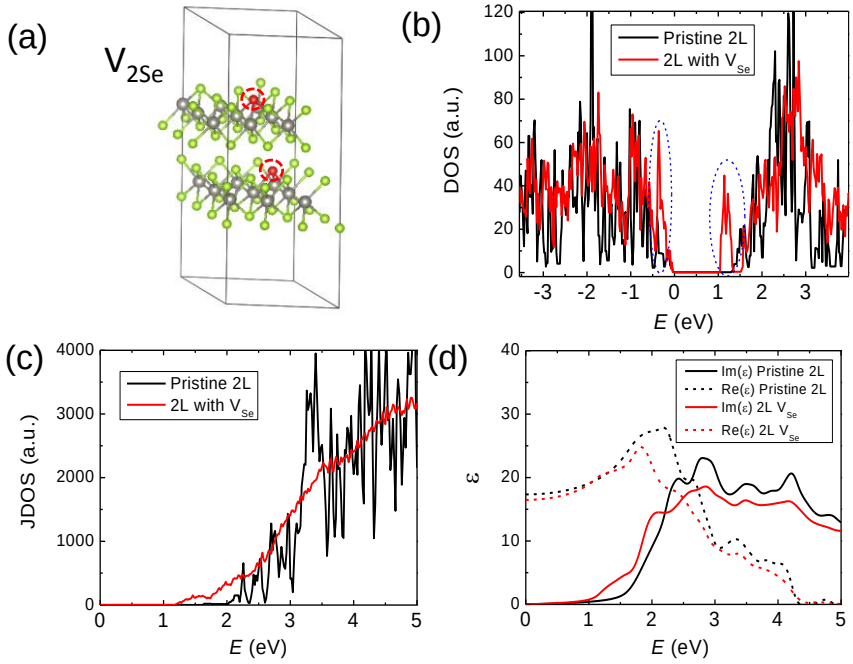

Fig. S3 (a) Atomic structure of 2L WSe_2 in 3×3 unitcell with two Se vacancies. The two Se vacancies are simulated here assuming FIB ions will penetrate the first layer and cause the same bulk defect density as the single-layer one. (b) Calculated density of states (DOS), (c) joint density of states (JDOS) and (d) permittivity. Compared with single vacancy, slightly more changes are observed in both the JODS and permittivity.

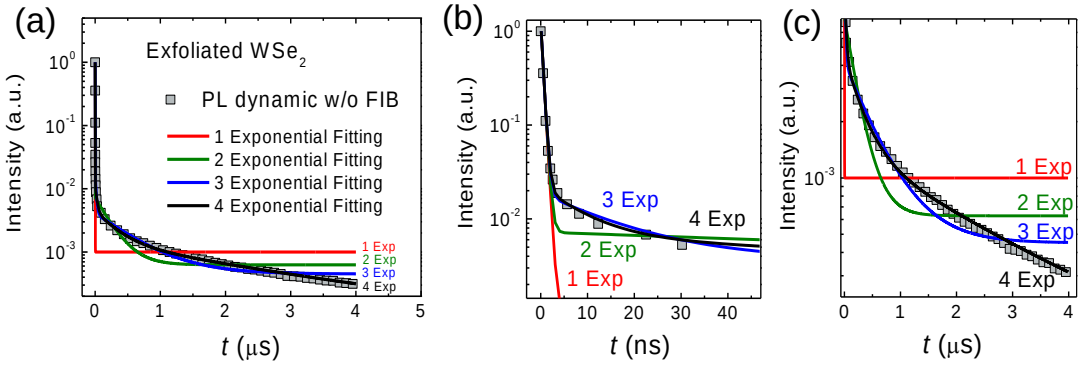

Fig. S4 Fitting of PL dynamics using exponential decays with different component number. The fitting equation is shown in equation *S1*, where A_0 is used to account for the background signal, A_i and τ_i are the decay amplitude and lifetime of exponential component i respectively, and n is the used total component number. (a) Fitting results for the PL dynamics of 1L WSe_2 without FIB, using 1,2,3 and 4 exponential components. As can be clearly seen, 4 exponential components are the minimum requirement to achieve a satisfactory fitting. Because of the long-time decay. limited exponential components (i.e. 1,2,or 3 components) can only fit the fast decays with priority, and the added new exponential components can better fit the slow decay, as shown by the zoomed fitting results in (b) and (c).

$$I(t) = A_0 + \sum_{i=1}^{n} A_i e^{-t/\tau_i} \qquad \text{(S1)}$$

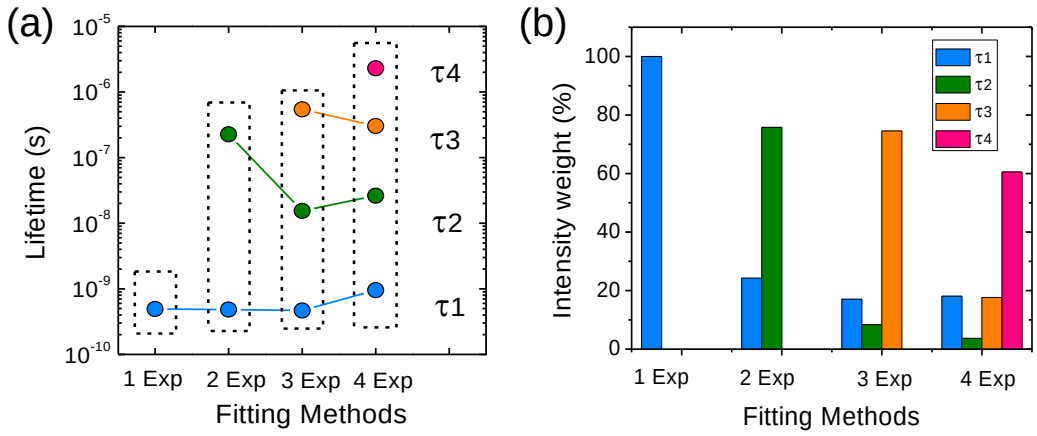

Fig. S5 (a) Extracted lifetime and (b) the corresponding intensity weights of different fitting methods with different exponential components. Because the least-square regression is

conducted in linear scale, fast decay is first fitted, as clearly reflected by the lifetime in (a). The slow decays are further revealed by the added exponential components.

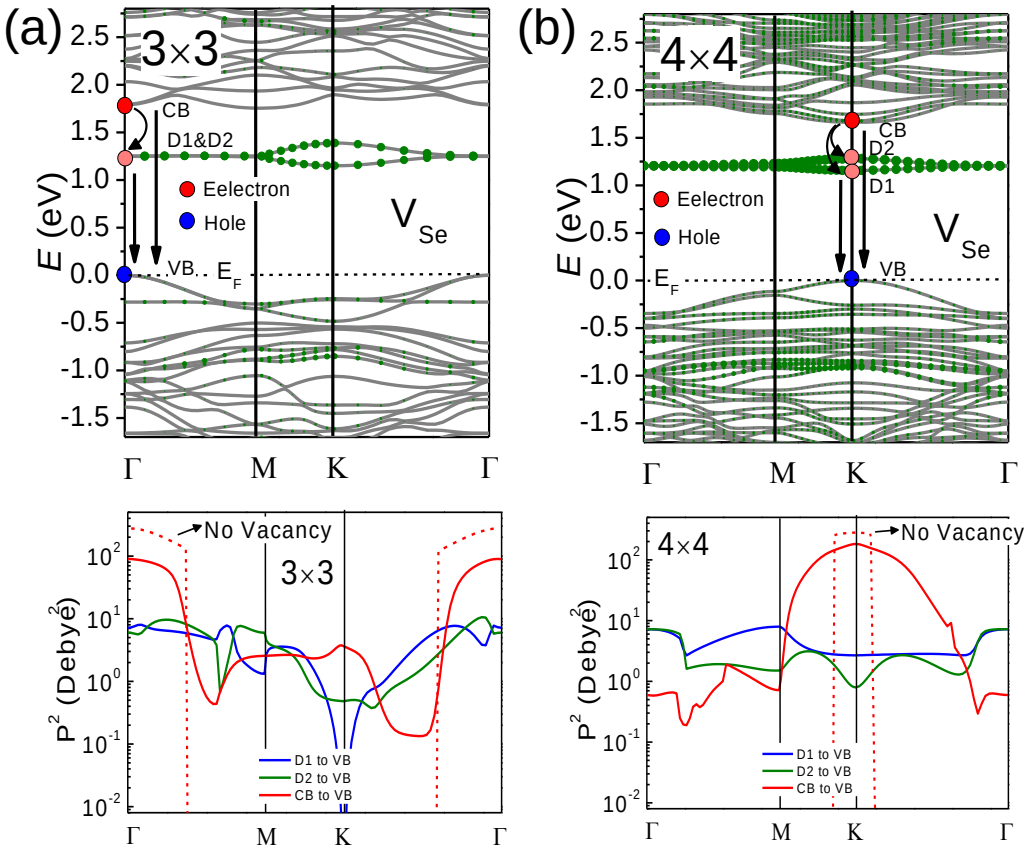

Fig. S6 Band structure and transition dipole moments of single-layer WSe_2 with Se vacancy calculated using (a) 3×3 supercell and (a) 4×4 supercell. Red dashed lines in the transition dipole moments are for transitions between conduction band and valence band of WSe_2 supercell with the same size but with no defects. Because of the Brillouin zone folding, bands with different k-points in 1×1 unitcell are now folded to the same k-point in the supercell, which causes the transition dipole moments for some k-points (the ones not near the bandgap) become zero in the supercell.

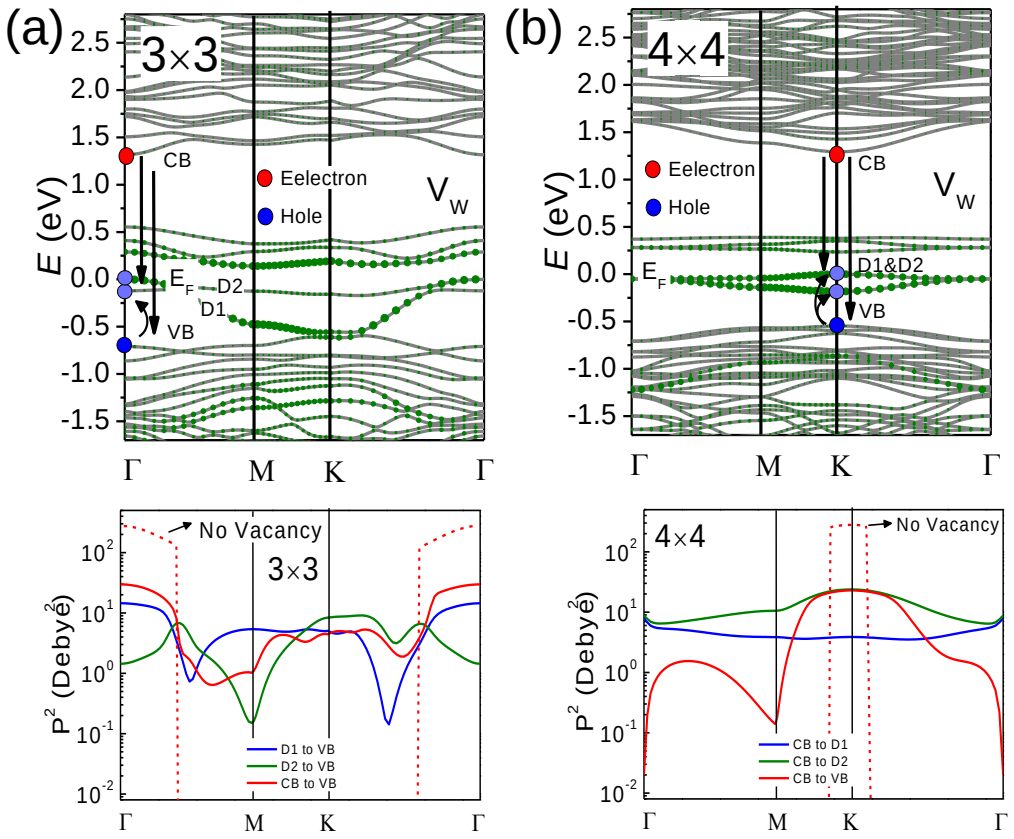

Fig. S7 Band structure and transition dipole moments of single-layer WSe_2 with W vacancy calculated using (a) 3×3 supercell and (a) 4×4 supercell. Red dashed lines in the transition dipole moments are for transitions between conduction band and valence band of WSe_2 supercell with the same size but with no defects.